ACS Sustainable Chemistry & Engineering

pubs.acs.org/journal/ascecg

Research Article

Dialdehyde Polysaccharides as Templates for Green Synthesis of Polypyrrole-Based Materials without Oxidative Polymerization

Jan Vícha,* Lukáš Münster, Filip Latečka, Martina Martínková, Zdenka Víchová, Ondřej Vašíček,* and Petr Humpolíček

Cite This: *ACS Sustainable Chem. Eng.* 2025, 13, 8435−8446

Read Online

ACCESS | Metrics & More | Article Recommendations | Supporting Information

ABSTRACT: Polypyrrole (PPy) is one of the most promising conductive polymers, with potential applications in energy storage, flexible electronics, and biomedicine. Broader use of PPy-based materials is, however, limited by harmful reactants used in their preparation and by the absence of strong interactions between relatively chemically inert PPy and the used matrices. Here, an innovative and green method is introduced based on a spontaneous condensation reaction between dialdehyde polysaccharides (DAPs) and pyrrole. The unique structure of DAPs spontaneously facilitates the chaining of pyrrole cycles into PPy copolymers without any added oxidizing agent or catalysts. This presents a new approach for preparing PPy-based materials with low cytotoxicity and strong antioxidative, anti-inflammatory, and immunomodulatory effects, ideal for biomedical applications. Moreover, this method can be combined with traditional oxidative polymerization to prepare covalently linked PPy composites with greatly improved resistance toward wear and loss of conductivity.

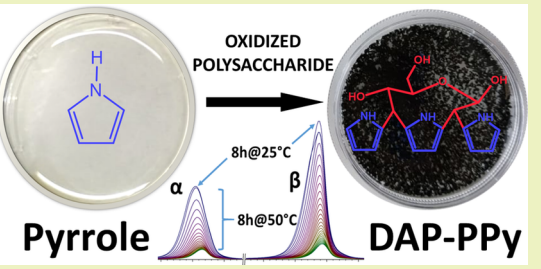

KEYWORDS: *polypyrrole, dialdehyde polysaccharides, conductive polymer, copolymer, composite*

1. INTRODUCTION

Polypyrrole (PPy) and its composites are receiving growing attention, particularly in the biomedical sector, mainly due to their biocompatibility, good conductivity under physiological conditions, promoting cell growth and differentiation, and accelerating wound healing processes.[1−5] PPy is also well suited for other applications, e.g., energy storage, wearable electronics, and the remediation of pollutants from the environment.[2] However, PPy-based materials have not yet been widely utilized due to several issues.

First, neat PPy is an inflexible, brittle, and poorly processable polymer. Producing uniform, defect-free PPy coatings is also challenging, particularly on nonconductive, irregularly shaped, or porous materials, where electrochemical polymerization cannot be utilized. In addition, although pure PPy is generally deemed biocompatible, its biocompatibility can vary depending on the synthesis methods and presence of residual monomers or dopants,[6] which may cause cytotoxicity, irritation, or inflammatory responses.

To mitigate the drawbacks of pure PPy, it is preferably utilized in the form of various composites. While composites allow improvement of some of the properties of PPy, they also have limitations. PPy composites are generally prepared by in situ oxidative polymerization of pyrrole in the presence of a suitable matrix. Part of the forming PPy is then adsorbed on the matrix surface or entrapped within its structure.[7] However, the relative chemical inertness of PPy means that it is bound to the matrix only by physical forces or weak interactions.[8] The absence of chemical bonds leads to poor adhesion of the conductive PPy layer to the matrix, its delamination, and leaching from the composite, particularly under repeated stress.[9] This causes loss of conductivity and may induce an adverse tissue reaction or immune response when PPy is used within biomaterials. The absence of bonds between PPy and the matrix is thus one of the main limitations of widespread utilization of PPy-based materials.

To introduce chemical bonds between the matrix and PPy, a two-stage procedure is usually employed. In the first step, pyrrole cycles are covalently attached to the matrix. In the second stage, pyrrole cycles bound to the matrix are incorporated into growing PPy chains during pyrrole's subsequent in situ polymerization.[10] This firmly binds the PPy layer to the matrix. However, current approaches to pyrrole anchoring are rather complex procedures that require labor-intensive methods, organic solvents, custom pyrrole derivatives, specialized linkers, and various toxic reactants.[11,12] For instance, to prepare conductive hyaluronate hydrogels with covalently incorporated PPy, Yang et al. used highly toxic 1-(cyanoethyl)-pyrrole, which had to be first reduced to N-(aminopropyl)-

Received: March 25, 2025
Revised: May 16, 2025
Accepted: May 16, 2025
Published: May 29, 2025

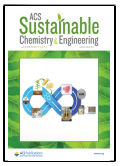

https://doi.org/10.1021/acssuschemeng.5c02711
ACS Sustainable Chem. Eng. 2025, 13, 8435−8446

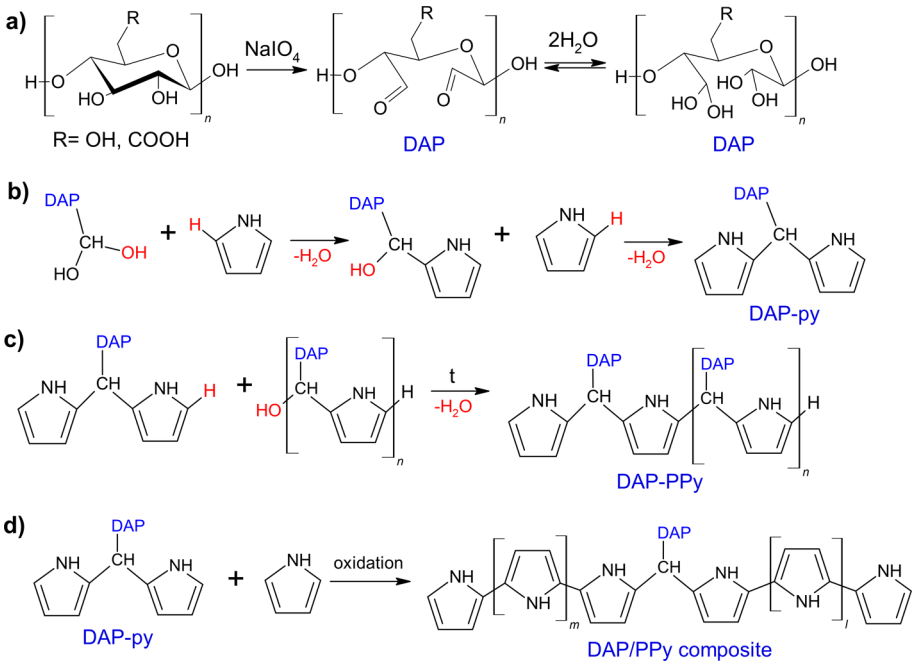

Figure 1. (a) General scheme of the oxidation of polysaccharides by $NaIO_4$. DAP is shown in its hydrated form (geminal diol), which is reversibly formed in aqueous solutions. (b) Scheme of an aldol condensation reaction between hydrated aldehyde groups of DAPs and pyrrole (py), leading to the formation of pyrrole-decorated DAP (DAP-py). (c) Scheme of copolymerization of DAP-py into DAP-PPy upon heating. (d) Scheme of DAP/PPy composite formation by oxidizing pyrrole in the presence of DAP-py.

pyrrole by $LiAlH_3$ in diethyl ether, then conjugated to hyaluronate by carbodiimide chemistry, and final conjugate dissolved in pyrrole solution and cross-linked by in situ oxidizing pyrrole to PPy.[11] The whole procedure is also substrate-specific to a large extent, as carboxylic groups must be present in the matrix.

Here, a novel, environmentally friendly, and straightforward method for the covalent pyrrole anchoring and fabrication of various PPy-based materials and composites is introduced. The method is based on a spontaneous aldol condensation reaction between pyrrole and dialdehyde polysaccharides (hereafter referred to as DAPs). DAPs, which serve as matrices and templates for pyrrole/PPy anchoring, are prepared by regioselective oxidation of various polysaccharides using sodium periodate ($NaIO_4$). During oxidation, a pair of adjacent hydroxyl groups is oxidized to reactive carbonyls upon simultaneous disruption of the carbon−carbon bond, see Figure 1a.[13] The preparation of DAPs is considered an environmentally friendly method due to the renewable nature of source polysaccharides and the possibility of regenerating $NaIO_4$ by green methods, such as ozone oxidation.[14] DAPs are also regarded as highly promising building blocks for fabricating advanced functional (bio)materials, primarily due to their rather unique poly-aldehydic character and significantly lower toxicity compared to low-molecular-weight organic dialdehydes.[13,15,16]

Presented spontaneous reaction between DAPs and pyrrole allows:

a) linker-free anchoring of pyrrole to DAPs (pyrrole-decorated DAPs are hereafter referred to as DAP-py, Figure 1b),
b) spontaneous chaining of bound pyrrole cycles into copolymers of DAP and PPy (hereafter referred to as DAP-PPy, Figure 1c), which is facilitated by the poly aldehydic character of DAPs and gentle heating without oxidative polymerization,
c) preparation of composites with covalently anchored PPy (hereafter referred to as DAP/PPy composite, Figure 1d), without toxic linkers, custom pyrrole derivatives, or organic solvents.

Besides the reaction mechanism and physical-chemical characterization of the products, the study focuses on extensive in vitro biological characterization of DAP-PPy, which exhibits very low cytotoxicity compared to PPy prepared by classical methods, as well as strong antioxidative, anti-inflammatory, and immunomodulatory effects.

2. METHODS

2.1. Synthesis and Characterization of DAP, DAP-py, DAP-PPy, and DAP/PPy Composites. The 2,3-dialdehyde cellulose (DAC), 2,3-dialdehyde hyaluronate (DAH), dialdehyde dextran (DADXA), and 2,3-dialdehyde alginate (DAAL), collectively termed dialdehyde polysaccharides (DAPs), were prepared following a general procedure: One gram of the source polysaccharide was dissolved (dispersed in the case of cellulose) in 50 mL of water and oxidized by sodium periodate in a 1.2 molar excess relative to the molar amount of oxidized units (see Table S1 for weights and concentrations of periodate) at 30 °C for 72 h (DAC) or 24 h (DAH, DAAL, DADXA) in the dark, following well-established procedures.[13] Insoluble DAC was purified by repeated centrifugation, solubilized for 2 h at 80 °C, and repurified by centrifugation and filtration.[17,18] All DAPs were subsequently thoroughly dialyzed against ultrapure water (UPW) for 72 h, followed by 48 h of dialysis against 0.05 M NaCl and another 24 h long dialysis against UPW to remove the salt, before being filtered and lyophilized. Fully oxidized DAPs contained the following CHO groups: DAC−12.5 mmol/g, DADXA−12.3 mmol/g, DAH−5.0 mmol/g, and DAAL−10.2 mmol/g. Differences in −CHO group content are caused by variations in the structure of source polysaccharides.[13] Oxidation was confirmed by infrared spectroscopy (Nicolet 6700 FT-IR, Thermo Fisher Scientific, USA), showing the presence of the C═O vibration of aldehyde groups (Figure S1a). The absence of residual iodine-based oxidants was confirmed by iodometry with UV−vis detection (Lambda 1050, PerkinElmer, USA) and by XRF spectroscopy; see Figure S1b,c.

https://doi.org/10.1021/acssuschemeng.5c02711
ACS Sustainable Chem. Eng. 2025, 13, 8435−8446

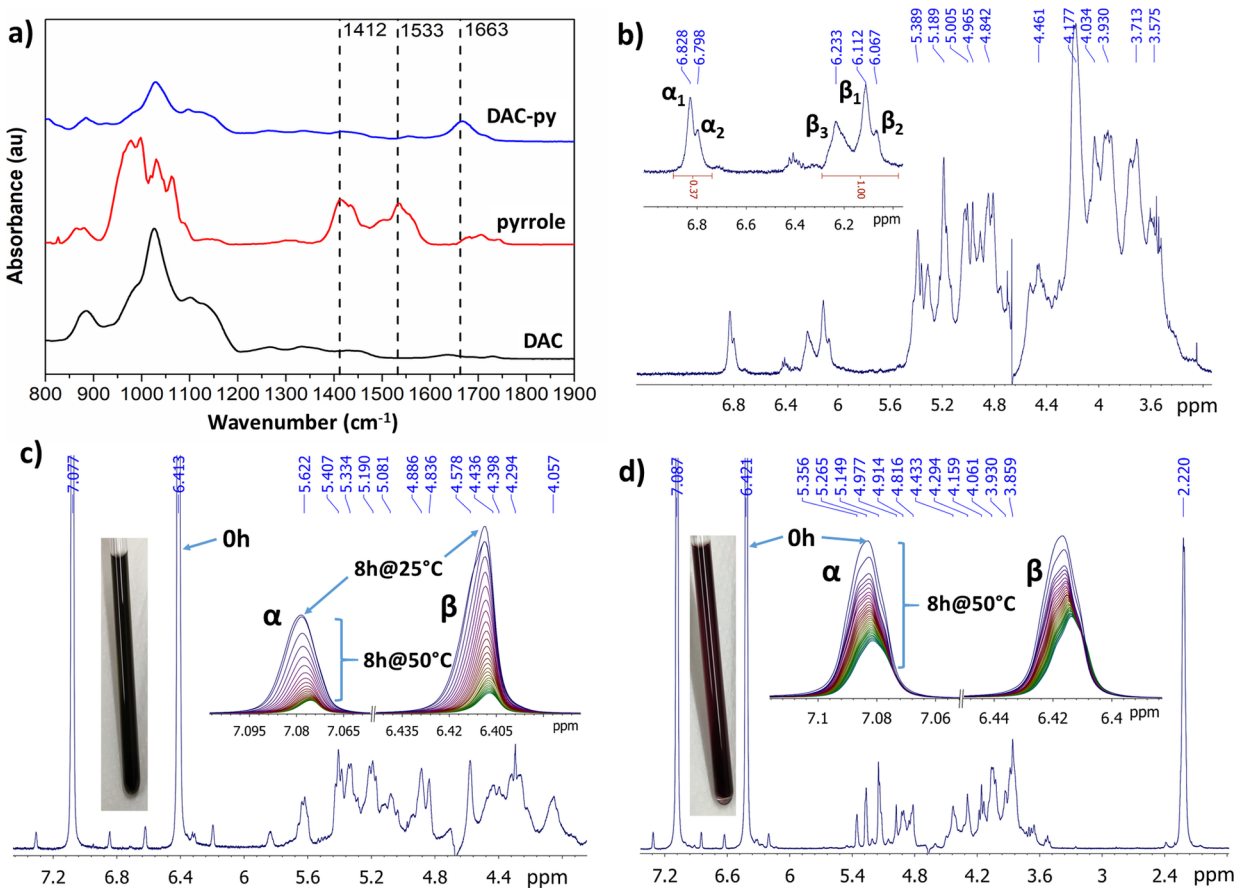

Figure 2. (a) FT-IR spectra of DAC pyrrole (py) and DAC-py showing the appearance of a distinct band at 1663 cm^{-1} after the binding of pyrrole. (b) ^{1}H NMR spectrum of DAC-py with a detail of pyrrole signals α and β (D_2O, 25 °C), where α designates the signals of H2/H5 protons and H3/H4 the signals of β protons of the pyrrole cycle. (c) ^{1}H NMR spectra of the DAAL/pyrrole mixture; 0 h—main spectrum; inset spectra—detail of py signals after 8 h at 25 °C and during 8 h of heating at 50 °C; photograph of the NMR tube after the measurement. (d) ^{1}H NMR spectra of the DAH/pyrrole mixture; 0 h—main spectrum, inset spectra—detail of py signals during 8 h of heating at 50 °C; photograph of the NMR tube after the measurement.

The ^{1}H NMR spectra of DAPs are given in Figure S2. Reaction yields were above 90% for DAH, DAAL, and DADXA, while additional purification and solubilization steps resulted in only 55% yield of DAC.

The molecular weight of DAP was determined using GPC with a RALS/LALS detector (see the SI for experimental details) and was as follows: DAC M_w = 7600 g/mol, PDI = 1.131, DAH M_w = 15,300 g/mol, PDI = 1.251, DADXA M_w = 40,100 g/mol, PDI = 2.303, DAAL M_w = 19,800 g/mol, PDI = 1.355.

In addition to the water-soluble DAPs, cellulose nanofibers (CNFs, 0.5 wt % suspension) were partially oxidized using 0.165 g of $NaIO_4$ per gram of CNFs (degree of oxidation, DO ~ 10%) for 72 h at 30 °C. The resulting dialdehyde cellulose nanofibers (DACNF) were purified by repeated centrifugation and dialysis as described above and used to prepare nanofibrous copolymers and composites.

To prepare the DAP-py (see Figure 1b), various amounts of pyrrole were added to the DAP solution (DAC, DAH, DAAL) in a molar ratio of n_{py}:n_{-CHO} of 1:1 or 2:1, respectively, where n_{py} is the molar amount of pyrrole and n_{-CHO} is the molar amount of DAP's—CHO groups. In the case of DAC, the reaction mixture was stirred overnight at 25 °C, purified by dialysis (UPW, 5 days), and lyophilized, and the final product (hereafter termed DAC-py) was redissolved in D_2O and studied by NMR. Reactions involving DAH and DAAL were performed directly in an NMR tube, and ^{1}H NMR spectra of DAH-py and DAAL-py were measured every 15 min (JEOL 400 MHz) to monitor the reaction progress.

To prepare DAP-PPy copolymers (see Figure 1c), a molar excess of pyrrole (final concentration of pyrrole 0.5 M, corresponding to an n_{py}:n_{-CHO} ratio between 8:1 for DAC and 20:1 for DAH, depending on n_{-CHO}) was added to a 5 mg/mL DAP solution or DACNF suspension (5 mg/mL). The pH was set to 3, and the mixture was heated to 50 °C (for soluble DAPs) or 70 °C (for DACNF) for 48 h. A pyrrole solution of the same concentration without DAP was used as a reference. Samples were purified by dialysis and lyophilized (DAP-PPy) or collected by filtration (DACNF).

Extreme care was taken to avoid contamination of the reaction mixtures with oxidizing agents that could initiate PPy polymerization. In addition to the thorough purification of DAPs by dialysis, freshly prepared ultrapure water (UPW) was used in all experiments, reactions were conducted in previously unused glassware rinsed with UPW, and only recently purchased, freshly opened chemicals of p.a. quality were used.

To prepare DAP/PPy composites (see Figure 1d), pyrrole was added to a DACNF suspension (5 mg/mL) in UPW, in a molar ratio of n_{py}:n_{-CHO} of 2:1 or 8:1 (final concentration of pyrrole 0.025 and 0.1 M), and the suspension was stirred for 24 h to allow for the formation of DAC-py on the surface of DACNF. Pyrrole polymerization was then initiated by adding $FeCl_3$ in a 1.65 molar excess relative to n_{py}, and the suspension was stirred at laboratory temperature for an additional 24 h. For comparison, analogous composites were prepared using non-oxidized CNFs following the same approach. The resulting composites were repeatedly washed with UPW, 0.2 M HCl, and ethanol and then lyophilized.

Further details of used materials, instrumentation, and biological evaluation are given in the Supporting Information.

2.1.1. Statistical Evaluation. Unless specified otherwise, all reported data are expressed as the mean ± standard error of the mean (n = 4), and data were statistically analyzed using one-way ANOVA followed by Dunnett's multiple comparison test (** $p < 0.01$).

https://doi.org/10.1021/acssuschemeng.5c02711
ACS Sustainable Chem. Eng. 2025, 13, 8435−8446

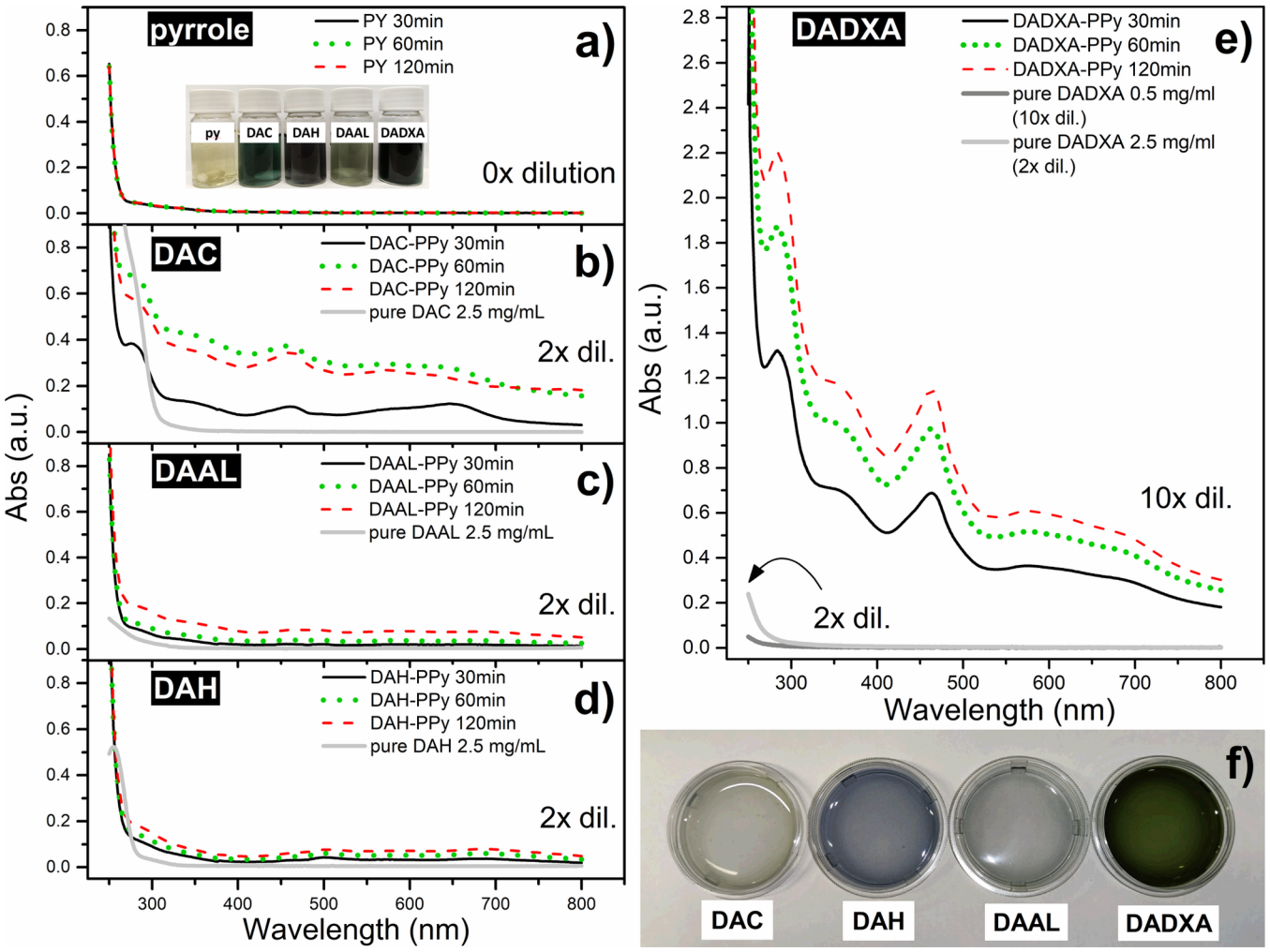

Figure 3. (a) UV−vis spectra of the reference pyrrole sample collected 30, 60, and 120 min after the reaction start and photograph of reaction vessels after 15 min of heating at 50 °C. (b, e) UV−vis spectra of DAC, DAAL, DAH, and DADXA (gray) and their colloids collected after 30, 60, and 120 min of heating (black, green, and red lines). Samples were diluted 2−10× due to strong absorptions, as indicated in the figure. (f) Photograph of samples after 24 h of heating.

3. RESULTS AND DISCUSSION

3.1. Pyrrole Spontaneously Reacts with DAP. The reaction between 2,3-dialdehyde cellulose (DAC) and pyrrole was initially investigated. The reaction was initiated by adding pyrrole to a DAC solution (n_{py}:n_{-CHO} of 1:1), followed by stirring overnight at laboratory temperature. Unbound pyrrole was removed by dialysis, and the final lyophilized product (DAC-py) was analyzed by FT-IR and NMR.

In FT-IR spectra, the binding of pyrrole to DAC was confirmed by the appearance of a new band at 1663 cm^{-1}, while the carbonyl group (C═O) vibrations of DAC at 1730 cm^{-1} disappeared, and the bands of pyrrole at 1533 and 1412 cm^{-1} shifted (Figure 2a).

The ^{1}H NMR spectra of DAC-py (Figure 2b) confirm the binding of pyrrole to DAC, as two sets of pyrrole signals around 6.8 ppm (H2, H5−marked as α signals) and between 6.0−6.25 ppm (H3, H4 of pyrrole−marked as β signals) were observed. The $^{1}H-^{13}C$ HSQC spectrum (Figure S3) correlated α signals with two ^{13}C resonances at ∼120.1 ppm and β with three ^{13}C signals between 107.5 and 108.7 ppm. Several different pyrrole binding modes are thus present in DAC-py. There are three possible reaction sites at the pyrrole cycle−nitrogen atom and carbon atoms in positions α and β. Because the lone electron pair of nitrogen is conjugated in the aromatic ring, the Schiff base reaction with aldehyde can be ruled out. Among α and β positions, β of pyrrole is significantly less reactive toward electrophiles than α. The reaction between pyrrole and aldehyde is thus most likely to occur at position α. Further analysis of the DAC-py ^{1}H NMR spectra confirmed this assumption. The intensity ratio of signals α:β is 0.37:1 instead of 1:1 found in neat pyrrole, which corresponds to the expected electrophilic substitution of the α proton(s) of pyrrole by the aldehyde, i.e., the aldol condensation reaction (Figure 1b).[19,20]

The aldol condensation is a two-stage reaction.[20] After the aldehyde binds to the first pyrrole cycle, the remaining −CH(OH)−group may still react with the second pyrrole cycle, which results in a pair of bound pyrrole cycles bridged by the −CH−group from DAC, see Figure 1b. Moreover, each pyrrole cycle has two α carbons and may thus react with two aldehyde groups. The observed 0.37:1 (α:β) signal ratio indicates that some pyrrole cycles are indeed bound by two aldehyde groups simultaneously. In other words, pyrrole thus may be bound to either C2 or C3 of DAC, or both.

To investigate the mode of pyrrole binding in DAC-py, $^{1}H-^{1}H$ COSY, $^{1}H-^{1}H$ TOCSY, and $^{1}H-^{13}C$ LR-HSQMBC[21]

https://doi.org/10.1021/acssuschemeng.5c02711
ACS Sustainable Chem. Eng. 2025, 13, 8435−8446

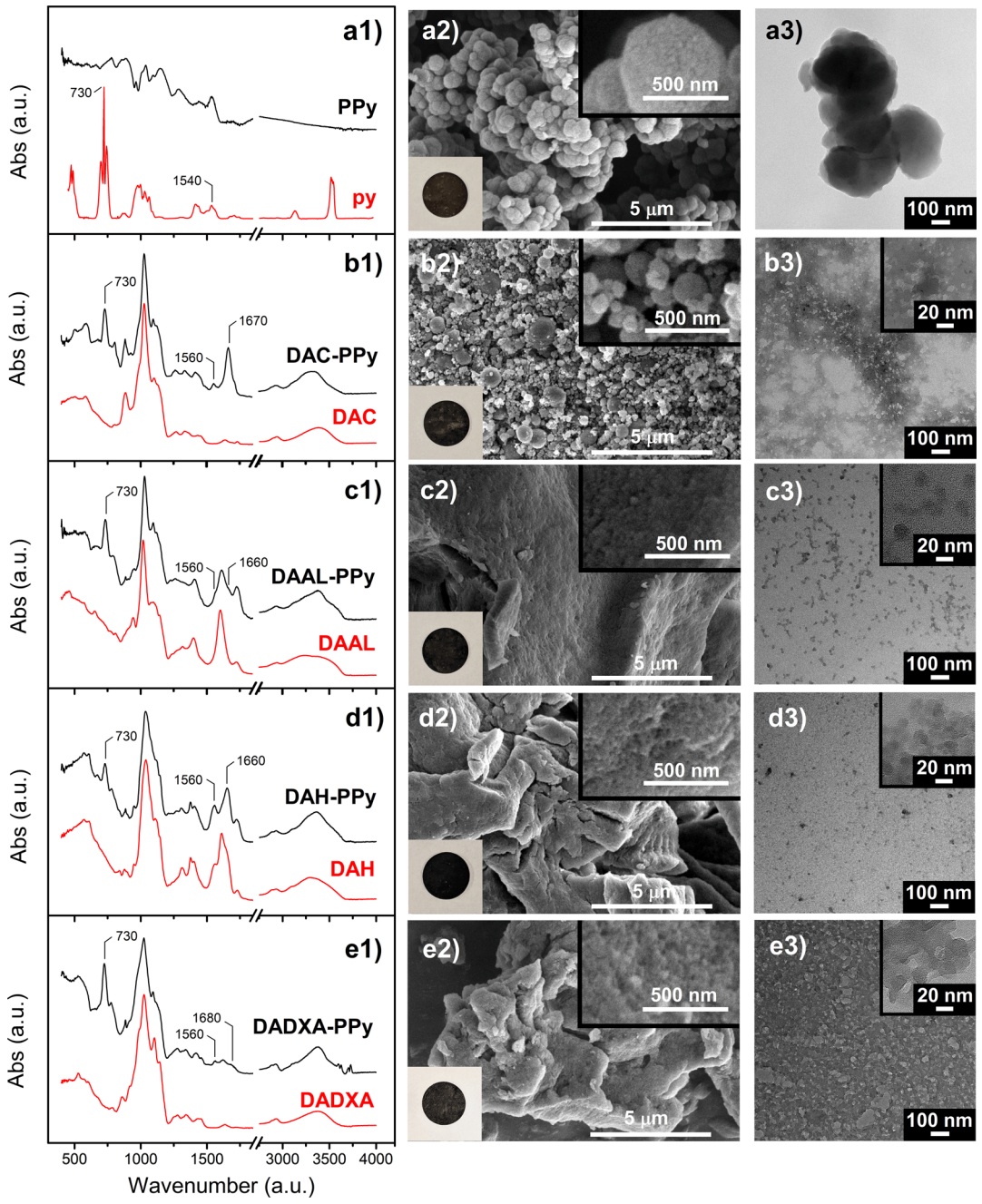

Figure 4. Column 1—FT-IR spectra of DAPs and their conjugates with PPy; Column 2—SEM micrographs with inset photographs of cylindrical specimens prepared from samples, Column 3—TEM micrographs of samples.

spectra were measured, see Figures S4—S7 in SI. Experimental details are given in SI.

The ^{1}H—^{1}H COSY and ^{1}H—^{1}H TOCSY (Figures S4 and S5 in SI) showed that the signal at 6.83 ppm (α_1) correlates with a signal at 6.11 ppm (β_1), while the α_2 signal at 6.80 ppm correlates with the β_2 signal at 6.07 ppm. ^{1}H—^{1}H COSY spectra also show a correlation between the β_3 signal and signals from DAC at 4.20 and 4.25 ppm but not with α signals. According to the ^{1}H—^{13}C LR-HSQMBC experiment (^{n}J = 8 Hz, Figure S6), the quaternary carbon signal at 126.1 ppm correlates with α_1/β_1, and the signal at 125.8 ppm correlates with the β_2 signal at 6.07 ppm. The second measured LR-HSQMBC spectrum optimized for measurement of very long-range correlations (^{n}J = 3 Hz, Figure S7) shows a weak seven-bond coupling between the β_1 signal of pyrrole at 6.12 ppm and the C6 carbon signal of DAC at 60.2 ppm.

Based on the performed experiments, it can be concluded that the two main types of single-substituted pyrrole cycles (still bearing the α proton) are present in DAP-py, each likely bound to a different aldehyde group (C2 or C3, respectively). Moreover, the β_3 signal at 6.23 ppm was tentatively assigned to pyrrole with both α protons substituted based on the absence of its correlations with α protons. However, due to weak signal intensities, signal overlap, and the complex structure of DAC-py, the exact structures of the DAC-py units cannot be unequivocally determined.

Nevertheless, results confirm that the spontaneous condensation reaction provides a convenient method for attaching

https://doi.org/10.1021/acssuschemeng.5c02711
ACS Sustainable Chem. Eng. 2025, 13, 8435—8446

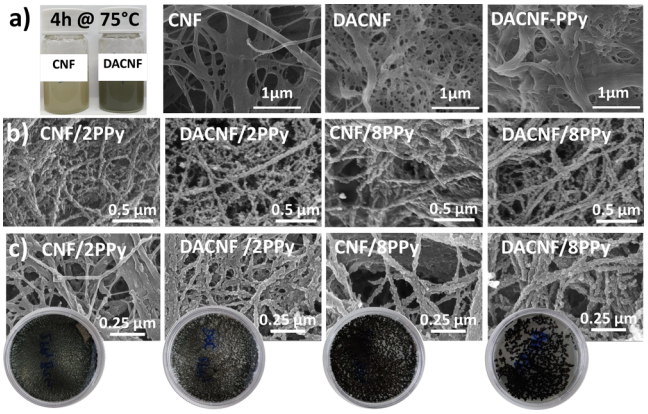

Figure 5. (a) CNF and DACNF suspensions after 4 h of heating in a pyrrole solution at 75 °C. SEM of CNF, DACNF, and DACNF-PPy. (b) SEM of CNF/2PPy, DACNF/2PPy, CNF/8PPy, and DACNF/8PPy. (c) SEM of CNF/2PPy, DACNF/2PPy, CNF/8PPy, and DACNF/8PPy after ultrasound treatment with inset photographs of Petri dishes showing the differences in bulk samples.

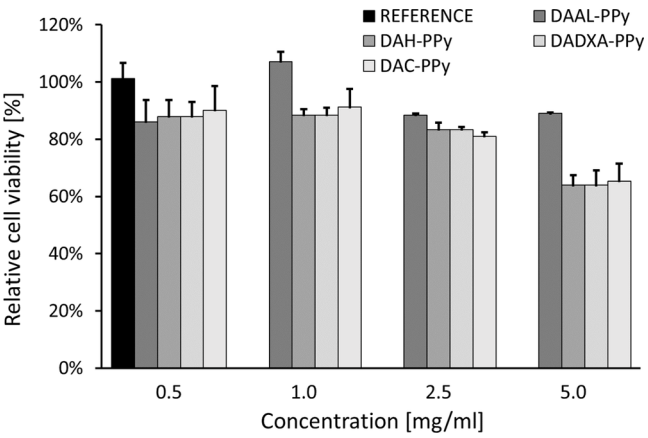

Figure 6. Cytotoxicity of DAP-PPy samples at different concentrations (0.5−5.0 mg/mL) toward mouse embryonic fibroblasts (NIH/3T3 cell line). The dashed line represents the cytotoxicity threshold according to ISO 10993−5. Data were converted to a percentage of the viability of cells incubated without samples and expressed as the mean ± standard error of the mean ($n = 4$). Data were statistically analyzed using one-way ANOVA followed by a two-sample t test with Bonferroni adjustment (* $p < 0.05$, ** $p < 0.01$).

pyrrole to DAP and could be used to modify oxidized cellulose surfaces or immobilize pyrrole-based compounds.

3.2. Heating of DAP-py Initiates Pyrrole Copolymerization. The ability of pyrrole to bind two aldehyde groups also indicates a very interesting possibility of spontaneous linking of pyrrole cycles along the DAC chains without any oxidizing agent.

To investigate, GPC analysis of the DAC-py sample was performed, and the results were compared with neat DAC. It revealed a significant increase in M_w of DAC-py (M_w = 32,900 Da, PDI = 1.088), four times higher than in free DAC (M_w = 7600 Da). Such an increase in M_w indicates the chaining of DAC molecules, likely via pyrrole cycles. Pyrrole, thus, may act as a cross-linker for DAC.

To investigate this further, a solution of DAC with an excess of pyrrole (n_{py}:n_{-CHO} 8:1) was heated directly in an NMR tube to 50 °C, which resulted in the rapid formation of a dark green precipitate. Although the color change suggested the formation of pyrrole (co)oligomers, NMR could not further analyze the insoluble precipitate. Instead, more soluble 2,3-dialdehyde alginate (DAAL) and 2,3-dialdehyde hyaluronate (DAH) were utilized. The reaction between pyrrole and DAAL or DAH was performed directly in NMR tubes (D_2O, n_{py}:n_{-CHO} ratio 1:1 for DAAL and 2:1 for DAH). The DAAL sample was initially incubated for 8 h at 25 °C to allow for the formation of DAAL-py, i.e., the decoration of DAAL with pyrrole. After 8 h at laboratory temperature, the intensity of the free pyrrole α signal at 7.08 ppm was reduced by 25% compared to β due to the aldol condensation reaction between pyrrole and DAAL, see the inset spectrum in Figure 2c. Next, the sample was heated to 50 °C in a spectrometer, and ^{1}H NMR spectra were measured every 15 min for 8 h. During this period, the pyrrole signals essentially disappeared from the spectra, and the red-black colloid was formed as a result of the pyrrole-DAAL chaining reaction (Figure 2c).

Next, the reaction of pyrrole with DAH (n_{py}:n_{-CHO} ratio 2:1) was studied. The NMR tube was heated to 50 °C, and time-resolved ^{1}H NMR spectra were recorded as before, see Figure 2d. The spectra showed a significant decrease in pyrrole signal intensities (faster for the α signal), accompanied by the broadening of DAH signals (Figure S8) and the formation of a purple-black colloid in the NMR tube (Figure 2e).

The abundance of aldehyde groups in DAPs thus facilitates the chain condensation of pyrrole cycles along the polysaccharide backbone (Figure 1c) and related cross-linking of the DAPs macromolecules, leading to the formation of colloids. The reaction rate is significantly increased by elevated temperature. The resulting materials are collectively referred to as DAP-PPy copolymers in the subsequent sections.

3.3. DAP-PPy Reaction Allows the Preparation of PPy-based Materials without Oxidative Polymerization. To further examine the reaction between DAP and pyrrole, the previously used DAPs, i.e., the DAC, DAH, and DAAL, complemented by 2,3-dialdehyde dextran (DADXA), were dissolved in UPW, and an excess of pyrrole was added (final c_{py} = 0.5 M). A solution of pyrrole without DAPs was used as a control. The pH of all solutions was adjusted to 3 to standardize the reaction conditions, protonate pyrrole bases, and catalyze the aldol condensation reaction.[20] All samples were subsequently heated to 50 °C. A color change, indicating the formation of DAP-PPy, was observed within minutes (Figure 3a). Interestingly, the reaction of DAC and DADXA resulted in emerald-colored colloids, while DAAL and DAH produced blue and purple ones, respectively. The color differences are likely due to the self-doping of pyrrole by the −COOH groups present in DAAL and DAH, see below.

UV−vis spectra of samples were collected after 30, 60, and 120 min (Figure 3a−e) to monitor the reaction progress. While no spectral changes were observed for the reference pyrrole solution (Figure 3a), the spectra of all DAP-PPy samples differ significantly from the spectra of neat DAPs (in gray). All DAP-PPy spectra show a typical absorbance of the conjugated pyrrole cycles between 450−500 nm, corresponding to the $\pi-\pi^*$ transition from the valence to the antibonding band due to the presence of the polaron.[22] Spectra of DADXA-PPy and DAC-PPy also contain additional absorbances between 250−400 nm, likely responsible for their green color. The highest increase in UV−vis absorbance, corresponding to the fastest reaction, was found in the DADXA-PPy spectrum. After 120 min of heating, precipitation occurred in the DAC-containing sample, likely due to the lowest ability of DAC to stabilize forming particles, see

https://doi.org/10.1021/acssuschemeng.5c02711
ACS Sustainable Chem. Eng. 2025, 13, 8435−8446

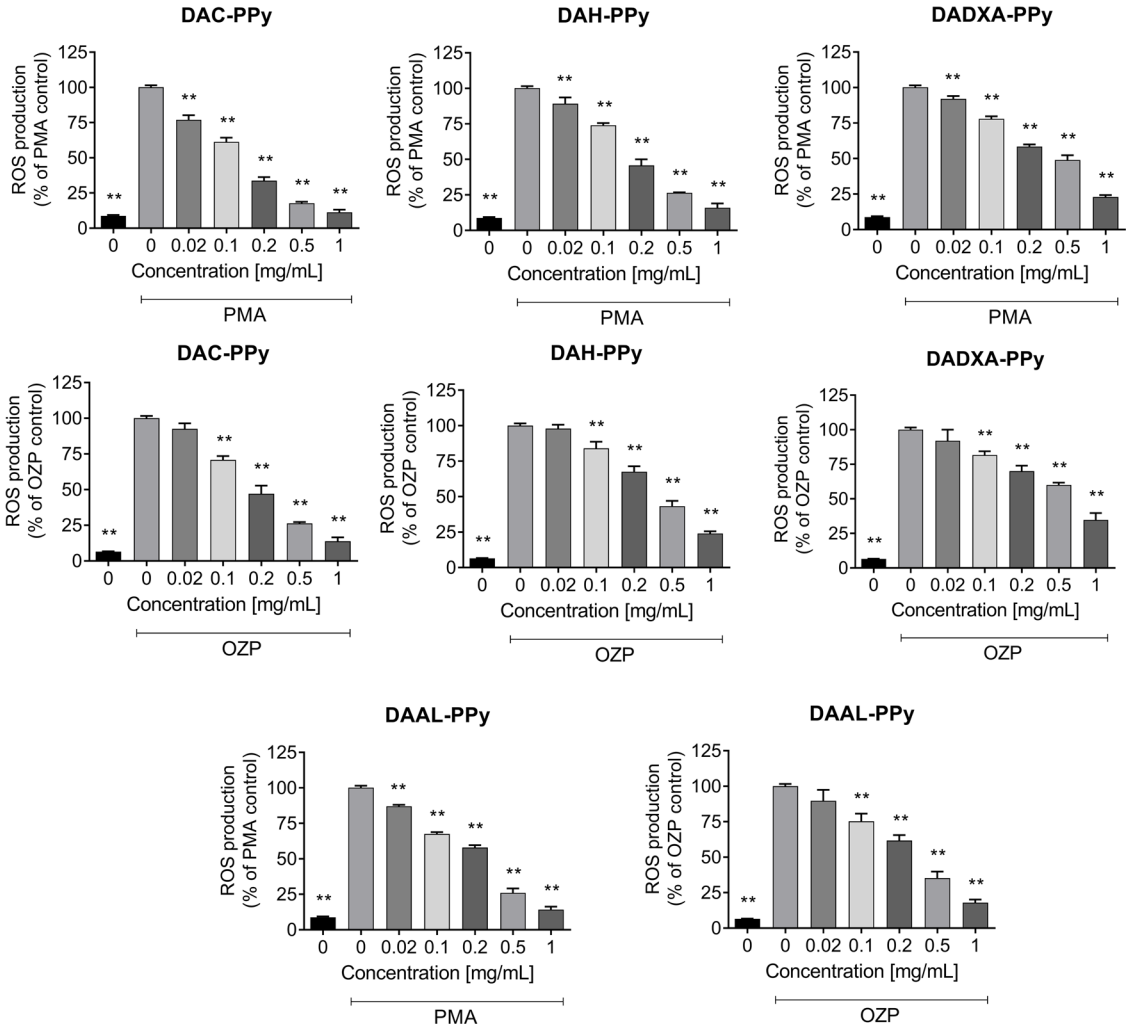

Figure 7. Effect of DAC-PPy, DAH-PPy, DADXA-PPy, and DAAL-PPy at different concentrations on ROS production by neutrophils, activated by PMA and OZP. Data were converted to a percentage of the relevant activated control (OZP or PMA and 0% of DAP-PPy).

below. After 24 h of heating, DAH and DAAL formed black colloids, while DAC and DADXA produced particle suspensions of dark-green color (Figure 3f). Only the reference pyrrole solution remained clear for the entire time (48 h), confirming that the reaction occurs only in the presence of DAPs. The samples were subsequently purified by dialysis, lyophilized, and further analyzed by FT-IR, SEM, and TEM. UV−vis spectra of the purified DAH-PPy and DAAL-PPy colloids are shown in Figure S9 in the SI. Three main absorbances are visible in the spectra (295, 485, and 590 nm for DAAL-PPy, and 298, 497, and 590 nm for DAH-PPy).

The FT-IR spectra of DAP-PPy (Figure 4) show vibrations from the source DAPs (−C−O−C−hemiacetal groups in the range of 1000−1200 cm^{-1}) and pyrrole cycles (C−H vibration at 730 cm^{-1} and C═C stretching vibration at 1560 cm^{-1}) as well as several new vibrations not present in the IR spectra of the original constituents. Among these, vibrations between 1660 and 1680 cm^{-1} are of particular interest as they are indicative of aldol condensation reaction and the formation of pyrrole−DAP bonds, as discussed already in Section 3.1.[4]

SEM and TEM analysis revealed spherical DAP-PPy particles (Figure 4b−e) with diameters in the range of 10−20 nm for DAH-PPy and DAAL-PPy and 100−200 nm in the case of DADXA-PPy and DAC-PPy. These are significantly smaller than particles of pure PPy prepared for comparison by $FeCl_3$ oxidation in the absence of DAPs (>500 nm, Figure 4a). The hydrodynamic radius (d_h), ζ-potentials, and polydispersity indices (PDI) of the particles according to DLS are $d_{h\ DAH\text{-}PPy} = 118 \pm 2$ nm, $\zeta_{DAH\text{-}PPy} = -30.8 \pm 4.1$ mV, $PDI_{DAH\text{-}PPy} = 0.327$; $d_{h\ DAAL\text{-}PPy} = 48 \pm 1$ nm, $\zeta_{DAAL\text{-}PPy} = -40.4 \pm 0.4$ mV, $PDI_{DAAL\text{-}PPy} = 0.392$; $d_{h\ DADXA\text{-}PPy} = 550 \pm 40$ nm, $\zeta_{DADXA\text{-}PPy} = 15.4 \pm 0.5$ mV, $PDI_{DADXA\text{-}PPy} = 0.720$; $d_{hDAC\text{-}PPy} = 870 \pm 80$ nm, $\zeta_{DAC\text{-}PPy} = -16.7 \pm 0.5$ mV, $PDI_{DAC\text{-}PPy} = 0.857$. DAAL-PPy thus had the smallest d_h of particles, followed by DAH-PPy, DADXA-PPy, and DAC-PPy. While DAH-PPy and DAAL-PPy have ζ-potentials between −30 and −40 mV, the ζ-potentials of DADXA-PPy and DAC-PPy were only about ±15 mV, which resulted in lower stability of their colloids, hence the observed precipitation. The observed differences between the ζ-potentials can be partially explained by the differences in the structure of DAPs, as they seem to scale with the content of anionic $-COO^-$ groups for DAAL and DAH. The differences between DAC-PPy and DADXA-PPy can be attributed to the lower amount of aldehyde groups and the oxidation-resistant branching anhydroglucose units in the latter; see our previous work for more details.[13] This is, however, difficult to determine exactly, as many other factors, from the size of particles to the protonation of pyrrole bases, may influence ζ-potentials.

https://doi.org/10.1021/acssuschemeng.5c02711
ACS Sustainable Chem. Eng. 2025, 13, 8435−8446

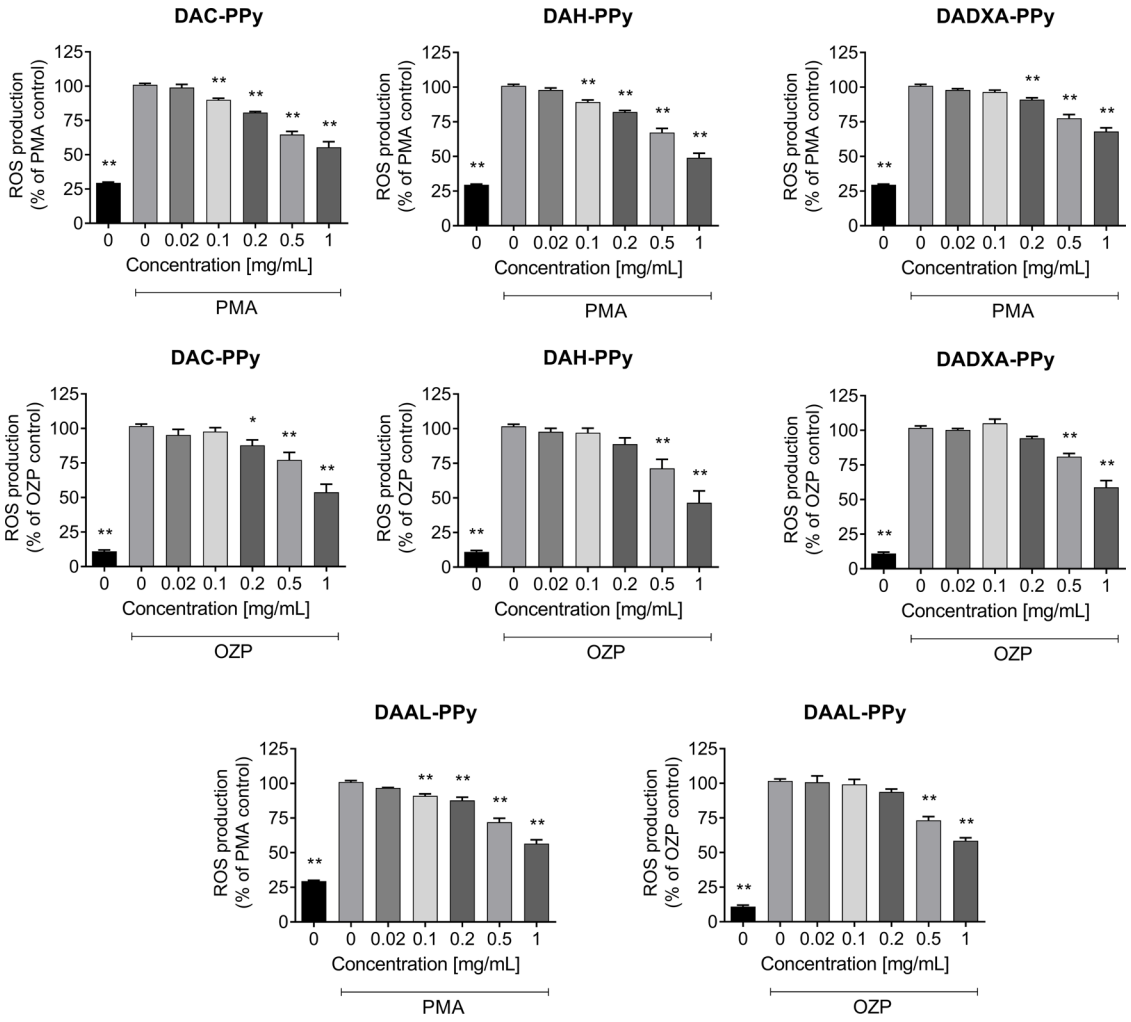

Figure 8. Effect of DAC-PPy, DAH-PPy, DADXA-PPy, and DAAL-PPy at different concentrations on PMA-activated and OZP-activated ROS production by 10× diluted whole blood. Data were converted to a percentage of the relevant activated control (OZP or PMA and 0% of DAP-PPy).

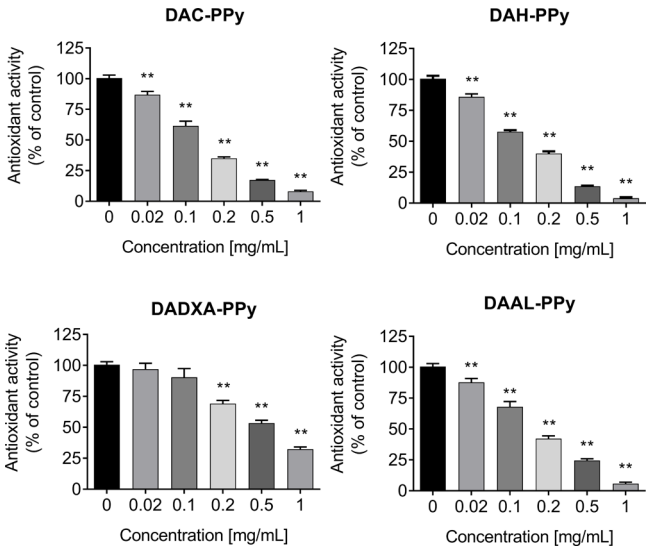

Figure 9. Antioxidant activities of DAC-PPy, DAH-PPy, DADXA-PPy, and DAAL-PPy at different concentrations of PPy particles. Data were expressed as a percentage relative to 0% DAP-Ppy (reference) and are presented as the mean ± standard error of the mean (n = 3).

Additional experiments were performed in NMR tubes to investigate the efficacy of the reaction. Two times molar excess of pyrrole (relative to n_{CHO} of the given DAP) was added to the NMR tube containing 10 mg of DAP dissolved in D_2O with 20% of DMSO-d_6. ^{1}H NMR spectra were measured immediately after the pyrrole addition and after 48 h at 50 °C. Intensities of the pyrrole β signal were compared to the signal of residual protons in DMSO-d_6 after 0 h and after 48 h at 50 °C to determine the percentage of pyrrole used during the reaction and, thus, the reaction yield. Signal β was used because it does not participate in the aldol condensation reaction. DMSO-d_6 was used as a reference due to its high boiling point, relative chemical inertness concerning the used compounds, and suitable chemical shift (2.5 ppm). ^{1}H NMR spectra are given in Figure S10. Over 99% of pyrrole was consumed in the case of DAC, DADXA, and DAAL, and 84% in the case of DAH. The reaction efficacy is thus very high. Crude DAC, DADXA, and DAAL colloids thus contain, on average, four pyrrole cycles per polysaccharide unit, while DAH contains approximately 3.4 pyrrole cycles per disaccharide unit. However, these values correspond to crude and unpurified colloids in which part of the unreacted pyrrole might be entrapped within the formed nanoparticles. Therefore, samples were purified by dialysis against water for 5 days and then lyophilized. Total yields of purified colloids were 47% for DAC-PPy, 49% for DAAL-PPy,

https://doi.org/10.1021/acssuschemeng.5c02711
ACS Sustainable Chem. Eng. 2025, 13, 8435−8446

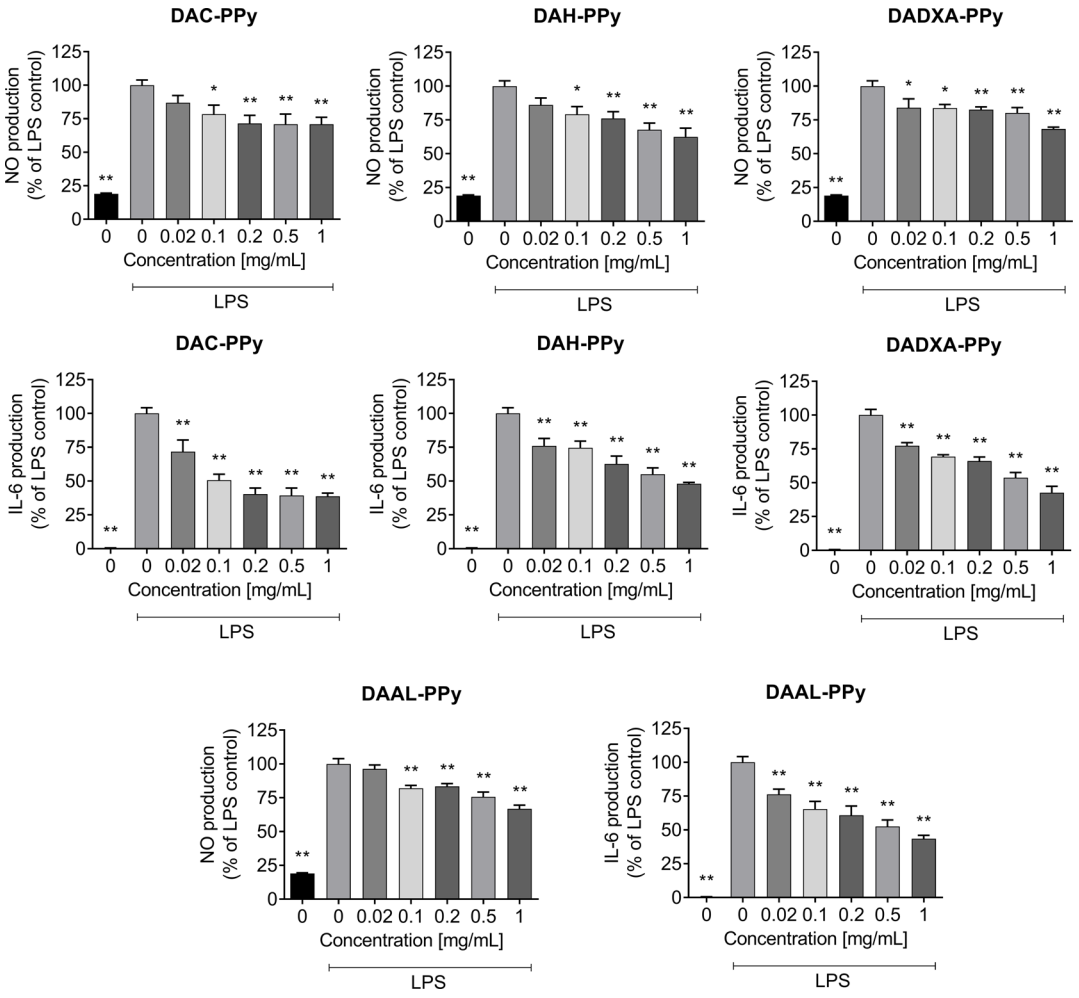

Figure 10. Effect of DAC-PPy, DAH-PPy, DADXA-PPy, and DAAL-PPy at different concentrations on NO production and IL-6 production by LPS-activated murine macrophages. Data were expressed as a percentage of the LPS-activated control (LPS and 0% of DAP-PPy).

31% for DAH, and 36% for DADXA. The purification of small-scale samples thus brings significant losses.

Next, the conductivity of the colloids was measured. Because the conductivity of lyophilized samples was very low due to the absence of dispersion media (see SI for more details), prepared DAP-PPy colloids and suspensions were purified by dialysis and ultrafiltration and redispersed in UPW at 0.1 mg/mL concentration. PPy colloid prepared without DAP (see discussion about Figure 4) served as a reference. Its conductivity was 8.6 μS/cm. Among DAP-PPy samples, DAH-PPy showed the highest conductivity (6.3 μS/cm), followed by the DAAL-PPy sample (3.9 μS/cm), DADXA-PPy (2.2 μS/cm), and DAC-PPy (1.8 μS/cm). The conductivities of all samples were comparable to those of the reference PPy colloid dispersed in UPW. The highest conductivities were obtained for both acidic polysaccharides, DAH and DAAL. Because the conductivity of PPy is dependent on the doping of pyrrole bases, it is assumed that both acidic polysaccharides, DAH and DAAL, can (at least partially) dope the pyrrole cycles due to the presence of COOH groups.

To summarize, heating of pyrrole/DAP solution can be used to prepare conductive DAP-PPy colloids (DAH-PPy and DAAL-PPy) or suspensions (DAC-PPy and DADXA-PPy) without the need for oxidative polymerization or stabilizers.

3.4. DAC-PPy Serves as a Template for the Preparation of Covalently Bound Composites. Following the study of soluble DAPs, cellulose nanofibers (CNFs) were used as a model of the insoluble template because cellulosic substrates are cheap, renewable, and widely used in medicine. Their modification is thus of high interest.

Initially, the CNFs were partially oxidized into the corresponding dialdehydes (DACNF, DO ~ 10%), purified, and heated for 48 h at 75 °C in a 0.5 M pyrrole solution at pH 3. Nonoxidized CNFs were treated in the same way and served as a reference. After several hours of heating, the gray-green color appeared for the DACNF-PPy sample, while the CNF sample remained mostly unchanged (Figure 5a). The reaction was slower than in the case of DAC-PPy, likely due to the lower amount of −CHO groups (lower DO). After the purification and isolation of DACNF-PPy, SEM analysis was performed. The nanofibrous structure of the CNFs was preserved after the oxidation to DACNF. Rib-like features also appeared on the surface of DACNF-PPy after heating (DACNF-PPy), likely due to the DAC-PPy layer.

The facile decoration of DACNF by pyrrole without the need for specialized linkers opens the possibility of preparing composites with covalent bonds between the matrix (DACNFs) and PPy, henceforth referred to as DACNF/PPy.

To prepare DACNF/PPy composites, DACNF suspensions were incubated in the presence of pyrrole (n_{py}:n_{-CHO} ratios of 2:1 or 8:1) for 24 h before initiating in situ oxidative polymerization by adding an excess of $FeCl_3$. During this

https://doi.org/10.1021/acssuschemeng.5c02711
ACS Sustainable Chem. Eng. 2025, 13, 8435−8446

procedure, pyrrole cycles that spontaneously reacted with DACNFs during the initial incubation period are incorporated into growing PPy chains, firmly binding the whole composite together by covalent bonds; see Figure 1d. For comparison, analogous composites were prepared using nonoxidized CNFs. SEM analysis (Figure 5b) of the resulting DACNF/2PPy, DACNF/8PPy, CNF/2PPy, and CNF/8PPy composites (numbers in sample names correspond to n_{py}:n_{-CHO} ratio used during the synthesis) revealed the presence of PPy grains deposited on the nanofibers. The PPy layer is visibly thicker in 8PPy samples due to the higher amount of PPy used during the synthesis.

To demonstrate the advantages of covalent anchoring of the PPy layer in DACNF, samples were subsequently homogenized for 30 min using a Bandelin Sonoplus HD2070 ultrasound homogenizer equipped with a titanium ultrasound needle MS 73 in water and without cooling to introduce wear. The comparison of samples after treatment is given in Figure 5c (in Petri dishes). SEM analysis revealed significant delamination of the PPy layer in samples prepared using nonoxidized CNF compared to DACNF samples, compare micrographs in Figure 5b,c. This is particularly evident in the CNF/2PPy sample, where the PPy layer seems almost absent compared to DACNF/2PPy. Partial delamination of the PPy layer is also visible in CNF/8PPy compared to DACNF/8PPy. Unfortunately, we could not directly quantify the delamination due to the fragmentation of the whole sample, particularly in CNF-based samples (Figure 5c). Nevertheless, the observed delamination of the conductive layer was reflected in the conductivities of the CNF/PPy and DACNF/PPy nanofibrous composites. The CNF/PPy samples initially showed higher conductivity than the DACNF/PPy samples, likely due to the absence of aliphatic −CH− bridges between bound pyrrole cycles, which partially disrupt the conjugated π-system and polaron propagation in DACNF/PPy. However, the advantage of covalent binding became apparent when composites were exposed to simulated wear using an ultrasound homogenizer. While the conductivity of CNF/2PPy decreased by 40% after the ultrasound treatment (from 0.32 to 0.19 mS/cm), and the conductivity of CNF/8PPy even by more than 70% (from 0.35 to 0.097 S/cm), the conductivity of DACNF/2PPy only decreased by 5% (from 0.060 to 0.056 mS/cm). The conductivity of DACNF/8PPy decreased by 24% (from 0.057 to 0.043 S/cm).

The use of DACNF-PPy as a composite matrix thus significantly mitigated the loss of conductivity typically associated with wear in the composites. Although further research is needed, this suggests that covalent PPy anchoring was successful and resulted in enhanced durability and performance of the composite materials.

3.5. DAP-PPy are Noncytotoxic, Antioxidative, and Anti-Inflammatory. Biological evaluation of the prepared materials began with testing the cytotoxicity of DAP-PPy samples on NIH/3T3 mouse embryonic fibroblasts, following ISO standard 10993−5:2009, which defines a cytotoxic effect as a reduction in cell viability by 30% relative to a reference standard (cells incubated without samples), see Figure 6.

DAC-PPy, DAH-PPy, and DADXA-PPy showed mild cytotoxicity only at the highest tested concentration of 5 mg/mL, while DAAL-PPy remained noncytotoxic even at this concentration. The cytotoxicity of all DAP-PPy samples, particularly DAAL-PPy, is remarkably low compared with other PPy colloids. The lowest cytotoxicity of DAAL-PPy could be due to its relatively high negative ζ-potential, which may cause repulsion with cellular membranes. For comparison, PPy colloids prepared by common techniques and stabilized by sodium dodecyl sulfate (SDS) showed cytotoxicity at concentrations already above 19.4 μg/mL,[23] and PVP-stabilized PPy colloids became cytotoxic above 200 μg/mL.[22] The cytotoxicity of all DAP-PPy is thus more than one order of magnitude lower.

Following the cytotoxicity evaluation, the impact of DAP-PPy on the detectable amount of reactive oxygen species (ROS) produced by neutrophils after activation by PMA or OZP was investigated; see Figure 7. Extensive ROS production is often associated with inflammation and can damage surrounding tissues. Therefore, moderating excessive ROS generation is important, particularly in chronic inflammation.

In this scenario, DAP-PPy significantly mitigated ROS production of activated neutrophils at a concentration as low as 0.02 mg/mL. The highest antioxidant activity was observed for DAC-PPy and DAAL-PPy, with the lowest activity seen for DADXA-PPy, although the differences were minor. ROS production decreased linearly with increasing doses of DAP-PPy. At a 1 mg/mL concentration, ROS levels were similar to those produced by nonactivated neutrophils, especially for DAC-PPy and DAAL-PPy.

Given these promising results, ROS production quenching was also evaluated in cells isolated from whole human blood, providing more clinically relevant data; see Figure 8. In this case, all samples showed similar performance as observed with isolated neutrophils, significantly reducing ROS production at 0.1 mg/mL and higher concentrations.

Next, the antioxidant activity of DAP-PPy was tested using a luminol-horseradish peroxidase-H_2O_2 cell-free system, see Figure 9. All samples except DADXA-PPy showed statistically significant antioxidative activity at the lowest concentration of 0.02 mg/mL and more than 90% quenching of ROS at a dosage of 1 mg/mL, thus confirming the earlier results.

After the significant antioxidative potential of DAP-PPy was established, its effects on macrophages were studied. Specifically, the impact of DAP-PPy on macrophage viability (expressed as mitochondrial activity, Figure S11) and on the production of NO and IL-6 cellular messengers was evaluated. NO levels influence angiogenesis and modulate chemoattractant cytokines that initiate postwound inflammation, while IL-6 is a pro-inflammatory interleukin whose dysregulation is associated with chronic inflammation.

Tested samples have no significant impact on macrophage mitochondrial activity and, thus, their viability at the given concentrations (Figure S11). NO production was moderately reduced in activated macrophages above 0.1 mg/mL, although this reduction appears only partially concentration-dependent (Figure 10). The impact of DAP-PPy on IL-6 production is more pronounced. A statistically significant decrease is observable already at doses as low as 0.02 mg/mL. The highest decrease in IL-6 production was observed for DAC-PPy, which reduced IL-6 production by 50% at 0.1 mg/mL. Differences between other samples were minor, but all reduced IL-6 production by at least 50% at a 1 mg/mL dose.

To summarize, the biological evaluation revealed that all DAP-PPy (i) exhibit very low cytotoxicity compared to other PPy colloids, (ii) can quench free radicals produced by both neutrophils and macrophages, and (iii) can decrease the production of pro-inflammatory cytokines. Therefore, DAP-PPy has the potential to reduce the inflammatory response. Combined with its other properties, DAP-PPy has a high

https://doi.org/10.1021/acssuschemeng.5c02711
ACS Sustainable Chem. Eng. 2025, 13, 8435−8446

potential as a material for wound healing or for the preparation of conductive scaffolds.

4. CONCLUSIONS

The aldol condensation reaction between pyrrole and dialdehyde polysaccharides, prepared by the regioselective oxidation of cellulose, dextran, hyaluronan, and alginate, was described, and the reaction mechanism was investigated. The spontaneous reaction runs in an aqueous environment without catalysts, organic solvents, linkers, or specialized pyrrole derivatives. Heating of the reaction mixture initiates the chaining of bound pyrrole cycles along DAP chains, resulting in the formation of DAP-PPy copolymers without the need for initiation of oxidative polymerization. This presents a new and significantly more environmentally friendly procedure for preparing PPy-based materials compared to classic fabrication techniques.

Various (nano)materials can be prepared depending on the properties of DAPs. Soluble DAPs produce colloids or suspensions, while nanofibrous materials can be used as templates for preparing composites with a covalently bound PPy layer in combination with classic oxidative polymerization. While the conductivity of DAP-based composites is somewhat lower than that of nonoxidized matrices (up to 0.06 S/cm), they are much less prone to delamination of the PPy layer and loss of properties. For instance, simulated wear decreased conductivity as low as 5%, up to 8× lower than in PPy composites based on nonoxidized CNF.

The main applications of DAP-PPy are envisioned in biomedicine due to their very low cytotoxicity and significant antioxidative, immunomodulatory, and anti-inflammatory properties. The improved durability of composites suggests potential applications in other fields, particularly in sensors or flexible electronics.

To summarize, the presented approach offers a more sustainable, straightforward, and environmentally friendly alternative to traditional methods of preparation of PPy-based materials.

■ ASSOCIATED CONTENT

Data Availability Statement

Data are available upon request.

Supporting Information

The Supporting Information is available free of charge at https://pubs.acs.org/doi/10.1021/acssuschemeng.5c02711.

> Detailed description of materials and methods; FT-IR and XRF spectra of source materials; ^{1}H NMR spectra of source materials, NMR spectra of DAC-py and DAH-py; UV−vis spectra of DAH-PPy and DAAL-PPy colloids; NMR analysis of the reaction yield; conductivity of DAP-PPy colloids; and graphs of mitochondrial activity of macrophages (PDF)

■ AUTHOR INFORMATION

Corresponding Authors

Jan Vícha − *Centre of Polymer Systems, Tomas Bata University in Zlín, 760 01 Zlín, Czech Republic;* orcid.org/0000-0003-3698-8236; Email: jvicha@utb.cz

Ondřej Vašíček − *Institute of Biophysics of the Czech Academy of Sciences, 612 00 Brno, Czech Republic;* orcid.org/0000-0001-5892-0457; Email: ondrej.vasicek@ibp.cz

Authors

Lukáš Münster − *Centre of Polymer Systems, Tomas Bata University in Zlín, 760 01 Zlín, Czech Republic;* orcid.org/0000-0003-1643-2038

Filip Latečka − *Centre of Polymer Systems, Tomas Bata University in Zlín, 760 01 Zlín, Czech Republic*

Martina Martínková − *Centre of Polymer Systems, Tomas Bata University in Zlín, 760 01 Zlín, Czech Republic*

Zdenka Víchová − *Centre of Polymer Systems, Tomas Bata University in Zlín, 760 01 Zlín, Czech Republic*

Petr Humpolíček − *Centre of Polymer Systems, Tomas Bata University in Zlín, 760 01 Zlín, Czech Republic; Department of Fat, Surfactant and Cosmetics Technology, Faculty of Technology, Tomas Bata University in Zlín, 760 01 Zlín, Czech Republic;* orcid.org/0000-0002-6837-6878

Complete contact information is available at: https://pubs.acs.org/10.1021/acssuschemeng.5c02711

Author Contributions

J.V.−Experimental design, synthesis of DAP-py, DAP-PPy, NMR analysis, preparation of figures, writing of the manuscript, conductivity measurements, funding acquisition. L.M.−Synthesis of DAP, FT-IR, UV−vis, SEM, TEM analysis, writing. F.L.−NMR and GPC analysis, sample preparation. M.M.−Preparation of DACNF and their PPy composites, conductivity measurements, and writing. Z.V.−Evaluation of cytotoxicity, experimental design, writing. O.V.−Biological evaluation, antioxidation properties, evaluation of immunomodulatory action, writing. P.H.−Experimental design, experiment supervision, funding acquisition, writing.

Notes

The authors declare no competing financial interest.

■ ACKNOWLEDGMENTS

The authors gratefully acknowledge the support from the Czech Science Foundation project 24-11534S. The Centre for Polymer Systems Internal Development Project RP/CPS/2024-28/001, financed by the Ministry of Education, Youth and Sports of the Czech Republic, is acknowledged.

■ REFERENCES

(1) Zare, E. N.; Agarwal, T.; Zarepour, A.; Pinelli, F.; Zarrabi, A.; Rossi, F.; Ashrafizadeh, M.; Maleki, A.; Shahbazi, M.-A.; Maiti, T. K.; Varma, R. S.; Tay, F. R.; Hamblin, M. R.; Mattoli, V.; Makvandi, P. Electroconductive Multi-Functional Polypyrrole Composites for Biomedical Applications. *Appl. Mater. Today* **2021**, *24*, No. 101117.

(2) Sood, Y.; Singh, K.; Mudila, H.; Lokhande, P. E.; Singh, L.; Kumar, D.; Kumar, A.; Mubarak, N. M.; Dehghani, M. H. Insights into Properties, Synthesis and Emerging Applications of Polypyrrole-Based Composites, and Future Prospective: A Review. *Heliyon* **2024**, *10* (13), No. e33643.

(3) Maráková, N.; Boeva, Z. A.; Humpolíček, P.; Lindfors, T.; Pacherník, J.; Kašpárková, V.; Radaszkiewicz, K. A.; Capáková, Z.; Minařík, A.; Lehocký, M. Electrochemically Prepared Composites of Graphene Oxide and Conducting Polymers: Cytocompatibility of Cardiomyocytes and Neural Progenitors. *Mater. Sci. Eng., C* **2019**, *105*, No. 110029.

(4) Káčerová, S.; Muchová, M.; Doudová, H.; Münster, L.; Hanulíková, B.; Valášková, K.; Kašpárková, V.; Kuřitka, I.; Humpolíček, P.; Víchová, Z.; Vašíček, O.; Vícha, J. Chitosan/Dialdehyde Cellulose Hydrogels with Covalently Anchored Polypyrrole: Novel Conductive, Antibacterial, Antioxidant, Immunomodulatory, and Anti-Inflammatory Materials. *Carbohydr. Polym.* **2024**, *327*, No. 121640.

(5) Liu, Y.; Wu, F. Synthesis and Application of Polypyrrole Nanofibers: A Review. *Nanoscale Adv.* **2023**, *5* (14), 3606−3618.
(6) Humpolicek, P.; Kasparkova, V.; Pachernik, J.; Stejskal, J.; Bober, P.; Capakova, Z.; Radaszkiewicz, K. A.; Junkar, I.; Lehocky, M. The Biocompatibility of Polyaniline and Polypyrrole: A Comparative Study of Their Cytotoxicity, Embryotoxicity and Impurity Profile. *Mater. Sci. Eng. C-Mater. Biol. Appl.* **2018**, *91*, 303−310.
(7) Maity, S.; Chatterjee, A. Textile/Polypyrrole Composites for Sensory Applications. *J. Compos.* **2015**, *2015*, No. e120516.
(8) Johnston, J. H.; Kelly, F. M.; Moraes, J.; Borrmann, T.; Flynn, D. Conducting Polymer Composites with Cellulose and Protein Fibres. *Curr. Appl. Phys.* **2006**, *6* (3), 587−590.
(9) Kim, K.-G.; Park, G. H.; Agumba, D. O.; Kim, S. Y. *In-Situ* Measurement of Drying and Electrochemical-Cycling-Induced Mechanical Behavior and Delamination of Polypyrrole Electrodes for Energy Storage Applications. *Surf. Interfaces* **2022**, *34*, No. 102297.
(10) Pike, A. R.; Patole, S. N.; Murray, N. C.; Ilyas, T.; Connolly, B. A.; Horrocks, B. R.; Houlton, A. Covalent and Non-Covalent Attachment and Patterning of Polypyrrole at Silicon Surfaces. *Adv. Mater.* **2003**, *15* (3), 254−257.
(11) Yang, J.; Choe, G.; Yang, S.; Jo, H.; Lee, J. Y. Polypyrrole-Incorporated Conductive Hyaluronic Acid Hydrogels. *Biomater. Res.* **2016**, *20* (4), 31.
(12) Gan, D.; Han, L.; Wang, M.; Xing, W.; Xu, T.; Zhang, H.; Wang, K.; Fang, L.; Lu, X. Conductive and Tough Hydrogels Based on Biopolymer Molecular Templates for Controlling in Situ Formation of Polypyrrole Nanorods. *ACS Appl. Mater. Interfaces* **2018**, *10* (42), 36218−36228.
(13) Muchová, M.; Münster, L.; Vávrová, A.; Capáková, Z.; Kuřitka, I.; Vícha, J. Comparison of Dialdehyde Polysaccharides as Crosslinkers for Hydrogels: The Case of Poly(Vinyl Alcohol). *Carbohydr. Polym.* **2022**, *279*, No. 119022.
(14) Koprivica, S.; Siller, M.; Hosoya, T.; Roggenstein, W.; Rosenau, T.; Potthast, A. Regeneration of Aqueous Periodate Solutions by Ozone Treatment: A Sustainable Approach for Dialdehyde Cellulose Production. *ChemSusChem* **2016**, *9* (8), 825−833.
(15) Münster, L.; Capáková, Z.; Fišera, M.; Kuřitka, I.; Vícha, J. Biocompatible Dialdehyde Cellulose/Poly(Vinyl Alcohol) Hydrogels with Tunable Properties. *Carbohydr. Polym.* **2019**, *218*, 333−342.
(16) Kim, U.-J.; Lee, Y. R.; Kang, T. H.; Choi, J. W.; Kimura, S.; Wada, M. Protein Adsorption of Dialdehyde Cellulose-Crosslinked Chitosan with High Amino Group Contents. *Carbohydr. Polym.* **2017**, *163* (Supplement C), 34−42.
(17) Kim, U.-J.; Wada, M.; Kuga, S. Solubilization of Dialdehyde Cellulose by Hot Water. *Carbohydr. Polym.* **2004**, *56* (1), 7−10.
(18) Münster, L.; Vícha, J.; Klofáč, J.; Masař, M.; Kucharczyk, P.; Kuřitka, I. Stability and Aging of Solubilized Dialdehyde Cellulose. *Cellulose* **2017**, *24* (7), 2753−2766.
(19) Gu, C.-Z.; Feng, Y.-Q.; Liu, P.-P.; Meng, S.-X. Selective Synthesis of *β*-Unsubstituted Meso-Aryl Substituted Tripyrranes in Water. *J. Saudi Chem. Soc.* **2015**, *19* (2), 227−232.
(20) Geier, G. R., III; Lindsey, S. J. Investigation of Porphyrin -Forming Reactions. Part 1. Pyrrole + Aldehyde Oligomerization in Two-Step, One-Flask Syntheses of Meso-Substituted Porphyrins. *J. Chem. Soc. Perkin Trans. 2* **2001**, No. 5, 677−686.
(21) Williamson, R. T.; Buevich, A. V.; Martin, G. E.; Parella, T. LR-HSQMBC: A Sensitive NMR Technique To Probe Very Long-Range Heteronuclear Coupling Pathways. *J. Org. Chem.* **2014**, *79* (9), 3887−3894.
(22) Káčerová, S.; Víchová, Z.; Valášková, K.; Vícha, J.; Münster, L.; Kašpárková, V.; Vašíček, O.; Humpolíček, P. Biocompatibility of Colloidal Polypyrrole. *Colloids Surf. B Biointerfaces* **2023**, *232*, No. 113605.
(23) Vaitkuviene, A.; Kaseta, V.; Voronovic, J.; Ramanauskaite, G.; Biziuleviciene, G.; Ramanaviciene, A.; Ramanavicius, A. Evaluation of Cytotoxicity of Polypyrrole Nanoparticles Synthesized by Oxidative Polymerization. *J. Hazard. Mater.* **2013**, *250*−*251*, 167−174.

https://doi.org/10.1021/acssuschemeng.5c02711
ACS Sustainable Chem. Eng. 2025, 13, 8435−8446